Quantitative model for predicting the imbibition dynamics of viscoelastic fluids in nonuniform microfluidic assays

Yashwant Rawat, Sachit Kalia, and Pranab Kumar Mondal*
Department of Mechanical Engineering, Indian Institute of Technology Guwahati, Assam 781039, India

(Received 31 May 2021; accepted 2 November 2021; published 29 November 2021)

We develop a mathematical model to quantitatively describe the imbibition dynamics of an elastic non-Newtonian fluid in a conical (nonuniform cross section) microfluidic assay. We consider the simplified Phan-Thien-Tanner viscoelastic model to represent the rheology of the elastic non-Newtonian fluid. Our model accounts for the geometrical features of the fluidic assay, the key parameters affecting the rheological behavior of the fluid, and predicts the imbibition dynamics effectively. By demonstrating the temporal advancement of the filling length in the conical capillary graphically, obtained for pertinent parametric values belonging to their physically permissible range, we report an underlying balance between capillary and viscous forces during imbibition resulting in three distinct regimes of filling. Nonuniformity in the capillary cross section gives rise to an alteration in the viscous force being applied at the contact line (manifested through the alteration in shear rate) during the imbibition process, which upon maintaining a balance with the dominant capillary force results in three different regimes of filling. We believe that the present analysis has a twofold significance. First, this work will enhance the understanding of underlying imbibition dynamics of viscoelastic fluids (most of the biofluids exhibit viscoelastic rheology) in nonuniform fluidic pathways. Second, the developed model is of significant practical relevance for the optimum design of microfluidic assays, primarily used for sample diagnostics in biochemical and biomedical applications.

DOI: 10.1103/PhysRevE.104.055106

I. INTRODUCTION

The beneficial interests in the phenomenon of capillary imbibition are overwhelming, and this paradigm of fluid dynamics finds many biomicrofluidics based applications [1–5]. The underlying dynamics of the imbibition phenomenon is strongly modulated by the geometrical configuration of the flow path, wetting characteristics of the confining surfaces, and most importantly, by the interfacial dynamics of the contact line formed at the liquid-liquid-solid surface [2,3,6–13]. Probing into the fundamental understanding of the underlying imbibition dynamics in narrow fluidic confinements alongside the ubiquitous imbibition phenomenon in capillary-driven flow configuration in several relevant applications has motivated researchers to interrogate many problematic issues of the capillarity induced flow physics from experimental investigations as well as theoretical analysis [4,6,14,15]. Albeit scientific analysis and investigation on the subject of capillary filling dynamics started way back in the 1920s, research endeavor in this paradigm is continuing essentially to explore several intricate issues governing the capillary-driven imbibition nontrivially [16,17].

A large variety of biological fluids such as blood, synovial fluid, saliva, nasal fluid, DNA solution, which are commonly taken in microfluidic flow assays (MFAs) for their quick transportation, rapid testing, and efficient diagnostics, exhibit non-Newtonian fluid rheology and precisely show viscoelastic behavior [18–21]. It is worth mentioning here that the phenomenon of the capillary-driven imbibition, which mainly occurs in MFAs, results in an underlying balance between the viscous and surface tension forces [6]. Thus, a complex interplay between the viscous force, which is nontrivial pertaining to the flow of rheological fluids in narrow fluidic confinements, and the surface tension force seems to have controllability in manipulating the filling rate of the imbibed fluid in the pathways. To this end, several aspects, like surface wettability, surface structuring or heterogeneity (artificially textured ridges or posts), surface roughness-wettability coupling, and grafting the soft polymeric layer on the inner surfaces of the fluidic pathways, application of external fields are ventured to alter the balance between the aforementioned two forces, leading to a precise alteration in the filling dynamics [3,9,22–26]. Despite the controllability on the filling rate of both Newtonian as well as inelastic non-Newtonian fluids [4,9,14,23], achieved through maneuvering the imbibition dynamics by using the aforementioned existing techniques, quantitative description of how the conical capillary (capillary with nonuniform cross section) influences the imbibition dynamics of viscoelastic fluid and, consequently, affects the underlying filling phenomenon is sparsely available in the literature [27]. Although understanding of such a phenomenon through experimental investigations is of significant relevance, developing a mathematical model in describing the underlying capillary-driven imbibition of viscoelastic fluid in a conical capillary would benefit the microfluidics

*Corresponding author: mail2pranab@gmail.com; pranabm@iitg.ac.in

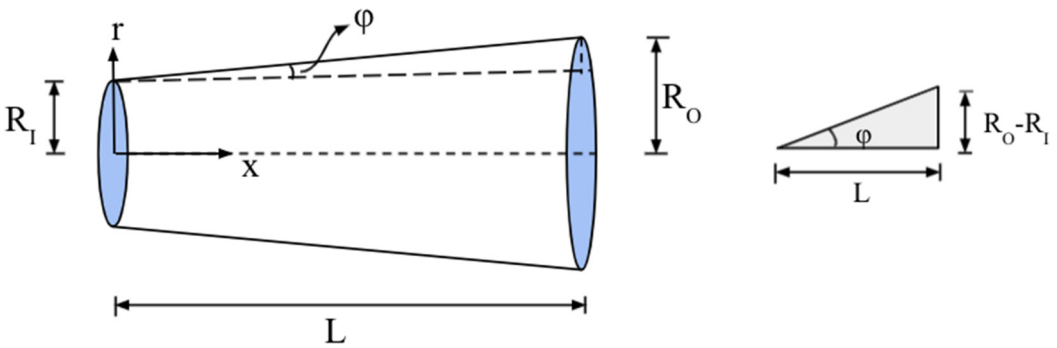

FIG. 1. Schematic diagram depicting the geometric configuration of the fluidic pathway considered in this study for the analysis. The dimensions of the fluidic channel are shown in the schematic. Coordinate system is attached at the center of the channel inlet. Taper angle of conical channel φ is shown at the right.

research community as well as the microfluidic flow assay developers.

Here, we propose a mathematical model to describe the imbibition dynamics of the viscoelastic fluid in a capillary having a nonuniform cross section. Our model considers the nonuniformity of the capillary cross section and takes the critical parameters of flow configuration (slight variation in capillary radius) as well as fluid properties into account. The present work is based on the assumption that the inner surface of the capillary is chemically as well as physically homogeneous and has a flat surface locally. We first scrutinize the effect of taper angle, characterizing the nonuniformity of the capillary on the imbibition dynamics and, subsequently, the focus is given to investigate the effect of fluid properties on the underlying filling process. Finally, we discuss the scaling laws to demarcate different regimes of filling and quantitatively describe the temporal variation of filling length in the capillary.

II. PROBLEM FORMULATION

As schematically depicted in Fig. 1, the problem considered in this study is the steady, unidirectional flow of an elastic non-Newtonian fluid through a narrow conical microfluidic channel. Here, the viscoelastic fluid is being filled under the influence of surface tension force only. We consider here the sPTT (simplified Phan-Thien-Tanner) model to represent the rheology of viscoelastic fluid [28,29]. For the present analysis, we consider the geometry of the fluidic channel with inlet radius R_{I} and outlet radius R_0. We denote the taper angle by φ. The coordinate system (cylindrical) for the analysis is also shown in the figure. The viscoelastic fluid being filled in this channel is considered to be free from any electrolytic behavior. Therefore, only the effect of surface tension force is acting as the driving force for the filling. Also, the Reynolds number is assumed to be small Re ($\ll 1$), ensuring the flow dynamics is analyzed in the laminar flow regime, which is typical to microscale transport [30,31].

The constitutive equation following the sPTT model is written as [28,32]

$$f(tr\boldsymbol{\tau})\boldsymbol{\tau}+\lambda\left[\frac{\partial\boldsymbol{\tau}}{\partial t}+\boldsymbol{u}\cdot\nabla\boldsymbol{\tau}-\left|(\nabla\boldsymbol{u})^T\cdot\boldsymbol{\tau}+\boldsymbol{\tau}\cdot\nabla\boldsymbol{u}\right|\right]=2\eta\mathbf{D} \tag{1}$$

The terms appearing in Eq. (1) are described as follows: $f(tr\boldsymbol{\tau})$ is a function of the trace tensor, τ is the stress tensor, η is the dynamic viscosity, λ is the relaxation time, and D is the deformation rate tensor.

Consistent with the assumptions as considered in this study, i.e., steady, unidirectional flow of viscoelastic fluid in the creeping flow regime, we obtain the simplified governing transport equation as given next. Pertaining to the present study, the elongational flow of viscoelastic fluid due to a divergent channel gives rise to the normal component of the stress in both r and x directions. However, on account of a small taper angle ($\varphi < 10^\circ$), the elongational flow due to normal stress in the r direction, i.e., τ_{rr}, can be neglected and the underlying flow is considered to be singularly dependent on the normal stress in the x direction, i.e., τ_{xx}. Thus, the flow in the divergent channel having a very small taper angle ($\varphi < 10^\circ$) can be considered essentially a unidirectional flow. The normal stress τ_{xx} depends on the shear stress τ_{xr}, and a relation between these two (τ_{xx} and τ_{xr}) can be constituted by simplifying the sPTT model as given in Eq. (1).

The function $f(tr\boldsymbol{\tau})$ for the linear sPTT model can be given as [33]

$$f(\tau_{kk})=1+\frac{\varepsilon\lambda\tau_{kk}}{\eta}. \tag{2}$$

Note that in Eq. (2), ε is the extensibility parameter. On simplification of Eq. (1) for steady and unidirectional flow, we arrive at the following equations [33]:

$$f(\tau_{kk})\tau_{xx}=2\lambda\frac{du}{dr}\tau_{xr}, \tag{3}$$

$$f(\tau_{kk})\tau_{rr}=0, \tag{4}$$

$$f(\tau_{kk})\tau_{xr}=\eta\frac{du}{dr}+\lambda\frac{du}{dr}\tau_{rr}. \tag{5}$$

From Eq. (4), we can set $\tau_{xx}=0$ as $f(\tau_{kk})=0$ gives a trivial solution [33]. Therefore, Eqs. (3) and (5) can be modified to the following form and given as [33]

$$\tau_{xx}=2\frac{\lambda}{\eta}\tau_{xr}^2, \tag{6}$$

$$f(\tau_{xx})\tau_{xr}=\eta\frac{du}{dr}. \tag{7}$$

Equation (6) gives the relation between the normal stress component τ_{xx} and the shear stress τ_{xr}. Now by making use of Eqs. (2), (6), and (7), we obtain the final differential form of the constitutive equation as [33]

$$\tau_{rx}\left(1+\frac{2\varepsilon\lambda^2{\tau_{rx}}^2}{\eta^2}\right)=\eta\frac{\partial u}{\partial r}. \tag{8}$$

Here ε is the extensibility parameter and u is the velocity of the fluid in the axial direction. This consideration of the small taper angle ($\varphi < 10^\circ$) of the capillary, alongside the assumption of unidirectional flow, leads us to obtain the fluid velocity only in the x direction.

The shear stress τ_{rx} in Eq. (8) is obtained from the Cauchy momentum equation, which for the assumptions considered pertaining to the present problem takes the following form:

$$-\frac{\partial P}{\partial x}+\frac{1}{r}\left(\frac{\partial(r\tau_{rx})}{\partial r}\right)=0. \tag{9}$$

Here, the pressure gradient $-dp/dx$ accounts for the cumulative effect of the forces participating in the actuation of the flow in the channel. In the present flow scenario, we consider two different forces to be present, *viz.,* the surface tension force and viscous force at the walls.

Also, the radius R is a function of x, and we denote it as $R(x) = R_I + \alpha x$. Note that in this relation, $\alpha = (R_O - R_I)/L$ where R_I and R_O are the inlet and outlet radius of the conical channel respectively, and L is the length of the channel. Therefore the taper angle φ can be given as $\varphi = \tan^{-1}\alpha$.

A. Hydrodynamics

For this problem, it is essential to establish the influence of the forces mentioned above on the flow velocity. In all our calculations, R is a function of x and their functional relationship is mentioned above. Using the symmetry condition at the center of the channel, i.e., at $r = 0$, we simplify Eq. (9) to obtain τ_{rx} as a function of r as given below:

$$\tau_{rx}=\frac{dP}{dx}\left(\frac{r}{2}\right). \tag{10}$$

Now, on employing the no-slip condition at the capillary walls ($u\,|_{r=R} = 0$), we solve Eq. (8) using Eq. (10) to obtain the velocity distribution. Below we write the velocity distribution as

$$u=\frac{dP}{dx}\left(\frac{r^2-R^2}{4\eta}\right)+\frac{2\epsilon\lambda^2}{\eta^3}\left(\frac{dP}{dx}\right)^3\left(\frac{r^4-R^4}{32}\right). \tag{11}$$

Note that in the above equation, R is a function of x and varies as $R(x) = R_I + \alpha x$.

On nondimensionalizing Eq. (11), we obtain a closed-form expression of velocity as given below:

$$\bar{u}=\overline{u_r}((1+\alpha\bar{x})^2-\bar{r}^2)+\delta\overline{u_r}^3((1+\alpha\bar{x})^4-\bar{r}^4). \tag{12}$$

Note that the parameters used for nondimensionalizing the above equation are

$u_r = -(\frac{R_I^2}{4\eta})\frac{\partial P}{\partial x}$, $t_{\text{ref}} = \sqrt{\frac{3R_I{}^3}{\gamma_s}}$, $\delta = \beta^2\sigma$, where $\beta = \sqrt{\frac{\gamma_s}{\rho R_I}}$, $\sigma = \frac{4\varepsilon\lambda^2}{R_I{}^2}$, and γ_s is the surface tension of the fluid.

Now, from Eq. (12), we obtain the expression of average velocity ($\overline{u_a}$) as

$$\overline{u_a} = -\frac{\alpha}{6}\overline{u_r}\,\{3+2\overline{u_r}^2\delta-6(1+\alpha\bar{x})^2[1+\delta\overline{u_r}^2(1+\alpha\bar{x})^2]\}. \tag{13}$$

The average velocity mentioned in Eq. (13) takes into account the effect of all the pertinent forces mentioned before. Now, we solve the cubic equation in $\overline{u_r}$ [Eq. (13)] to obtain the expression for $\overline{u_r}$. It is worthwhile to mention here that the expression of $\overline{u_r}$ is convoluted, and it is not given here for conciseness in the presentation. However, we here confirm to make this expression available upon request from the reader. It is worth mentioning here that we discard the complex roots of $\overline{u_r}$ while solving Eq. (13).

B. Capillary imbibition dynamics

In order to investigate the imbibition dynamics in the conical microfluidic assay, we use Newton's second law. Here, we assume a lump of fluid mass (control volume) in the fluidic channel being accelerated in the channel under the combined influences of surface tension and viscous forces. The lump is considered to have varying mass due to the continuous addition of mass in the lump. The amount of varying mass solely depends on the instantaneous rate at which the fluid is imbibed into the conical fluidic channel. So, we need to find the volume of a frustum of a cone at any temporal instant.

The volume of the lump can be calculated as

$$V = \tfrac{1}{3}\pi\left(3{R_I}^2+3\alpha R_I x+\alpha x^2\right)x, \tag{14}$$

where V is the instantaneous volume of the lump, R_I is inlet radii of capillary, and $\alpha = \tan\varphi$. Therefore, the momentum of the fluid mass can be written as

$$\rho V u_a = \tfrac{1}{3}\pi\left(3{R_I}^2+3\alpha R_I x+\alpha x^2\right)x\rho u_a. \tag{15}$$

Here ρ is the density of the viscoelastic fluid and u_a is the instantaneous average velocity of the fluid. Below we write the dimensional expression of the equation governing the fluid dynamics, to be precise imbibition dynamics of the present problem:

$$\frac{d}{dt}\left(\frac{1}{3}\pi\left(3{R_I}^2+3\alpha R_I x+\alpha x^2\right)x\rho u_a\right) = F_{\text{ST}}-F_v. \tag{16}$$

In Eq. (16), F_{ST} is the surface tension force and F_v is the viscous force. The expression for surface tension at a distance x from the inlet is given as

$$F_{\text{ST}} = 2\pi\gamma_s R(x)\cos\theta_s, \tag{17}$$

where θ_s is the contact angle of the fluid with the surface of capillary and γ_s is the surface tension coefficient of the fluid.

For calculating the viscous force F_v, we first calculate the expression of shear stress using Eq. (10) as

$$\tau_{rx}|_{r=R} = \frac{2\eta}{R}u_r. \tag{18}$$

In Eq. (18) R is a function of x. Therefore, viscous force takes the following form as

$$F_v=\int_0^x 2\pi R(x)\tau_{rx}|_{r=R}\,dx = 4\pi\eta u_r x. \tag{19}$$

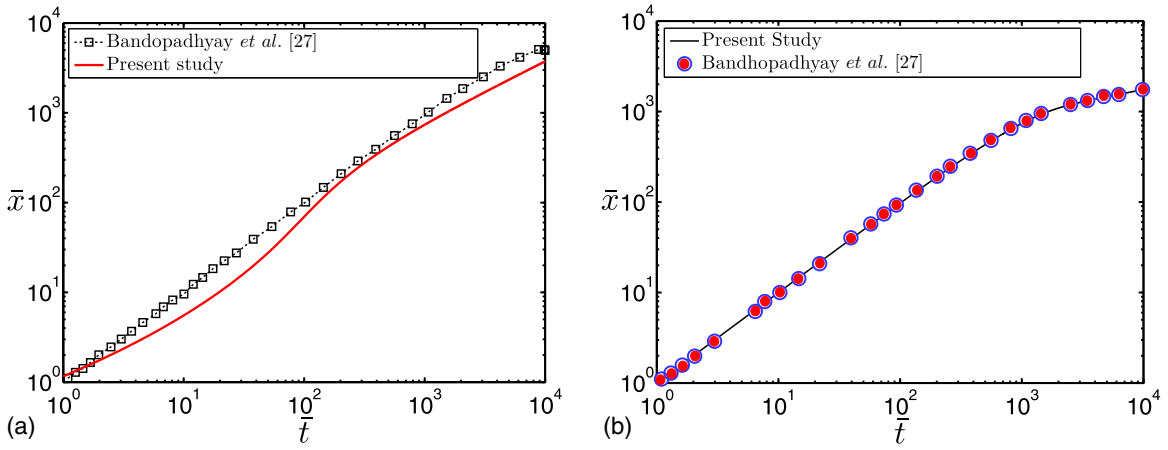

FIG. 2. (a) Plot showing the temporal variation of length of the liquid in the capillary. The solid line represents the results obtained from the present analysis while the markers are used to denote the reported results of Bandopadhyay *et al.* [27]. The other parameters considered are $\lambda = 0.1$ and $\varepsilon = 0.1$. A qualitative match between the present and published results is observed from the depicted plot in 2(a). (b) Plot showing the temporal variation of length of the liquid in the straight capillary. The results obtained from the present analysis pertaining to straight capillary are shown by solid line, and the markers are used to denote the reported results of Bandopadhyay *et al.* [27]. The other parameters considered are $\lambda = 0.01$ and $\varepsilon = 0.1$. A fairly accurate match between the present and published results is observed from the depicted plot in 2(b).

Substituting the values of F_{ST} and F_v, and using $u_a = \frac{dx}{dt}$, Eq. (16) can be simplified in the following form:

$$\frac{d}{dt}\left[\left(3{R_I}^2 x + 3\alpha R_I x^2 + \alpha^2 x^3\right)\frac{dx}{dt}\right] = \left(\frac{6\alpha\gamma_s\cos\theta_s - 12\eta u_r}{\rho}\right)x + \frac{6R_I\gamma_s\cos\theta_s}{\rho}. \quad (20)$$

We now take an effort to write Eq. (20) into its dimensionless counterpart form using the following reference parameters: $\bar{x} = \frac{x}{R_I}$, $\bar{\zeta} = \frac{R_I}{L}$, $\bar{t} = \frac{t}{t_{\text{ref}}}$, and $\beta = \sqrt{\frac{\gamma_s}{\rho R_I}}$. The dimensionless form of Eq. (20) reads as

$$\frac{d}{d\bar{t}}\left[\left(3\bar{\zeta}^2\bar{x} + 3\alpha\bar{\zeta}\bar{x}^2 + \alpha^2\bar{x}^3\right)\frac{d\bar{x}}{d\bar{t}}\right] = \left(6\alpha\cos\theta_s - \frac{12\eta\beta\overline{u_r}}{\gamma_s}\right)\bar{x} + 6\bar{\zeta}\cos\theta_s. \quad (21)$$

One can observe that Eq. (21) is a second-order nonlinear differential equation and does not have an exact solution. Hence, we solve Eq. (21) numerically by using the shooting method with accuracy up to the order 10^{-7}, subjected to the initial condition $\bar{x} = 0.0001$ and $d\bar{x}/d\bar{t} = 0$ at $\bar{t} = 0$. The solutions obtained are in the form of a Lagrange interpolation function that are further used to obtain the variation between $\bar{x}$ and $\bar{t}$. The variation is plotted for different pertinent cases, as discussed in detail, in the forthcoming sections.

III. MODEL VALIDATION

We here discuss the credibility of the present model in predicting the imbibition dynamics of viscoelastic fluid in the chosen fluidic configuration. In doing so, we stick to the dual benchmarking strategy discussed as follows. Since no work is available in the literature on the imbibition dynamics of viscoelastic fluid in the conical microfluidic pathway, we stick to validating our model for a limiting case. Pertaining to this task, we consider the imbibition dynamics of a viscoelastic fluid having its characteristic parameters $\lambda = 0.1$ and $\varepsilon = 0.1$, as reported in the literature [27], in a straight fluidic channel (which can be mimicked by tuning the taper angle in our model). Figure 2(a), which compares the temporal evolution of the filling length obtained from our model *vis-à-vis* the reported results [27], justifies our model's capability in calculating the filling length following the imbibition dynamics into the capillary.

It may be mentioned here that the difference, although not very significant, as observed from the depicted plots (between present and published results), is attributed to the variance in the geometrical configuration of the fluidic channel. Since the results reported in the literature [27] are obtained for a rectangular cross-section channel, for this validation as shown in Fig. 2(a), we consider the diameter of the tube in our analysis as the total height of the rectangular cross-section channel, considered in the referred study [27]. It is because of this reason that we observe a small difference in the results as witnessed in Fig. 2(a). Accounting for only the qualitative match between the present and published results, as seen in Fig. 2(a), we also take an effort in Fig. 2(b) to compare the filling length of the viscoelastic fluid, characterized by $\lambda = 0.01$ and $\varepsilon = 0.1$, in a straight capillary having a rectangular cross section as that considered in the reported analysis [27]. A fairly accurate match between the results of this analysis and the reported ones, as seen in Fig. 2(b) both qualitatively as well as quantitatively, justifies the credibility of the present modeling framework in predicting the filling length of the viscoelastic fluid being imbibed in the conical capillary.

IV. DISCUSSION OF THE IMBIBITION DYNAMICS

In this section, we shall discuss the imbibition dynamics of viscoelastic fluids in a conical microfluidic channel, as schematically shown in Fig. 1. To obtain the results, we consider several aspects, which encompass the fluid prop-

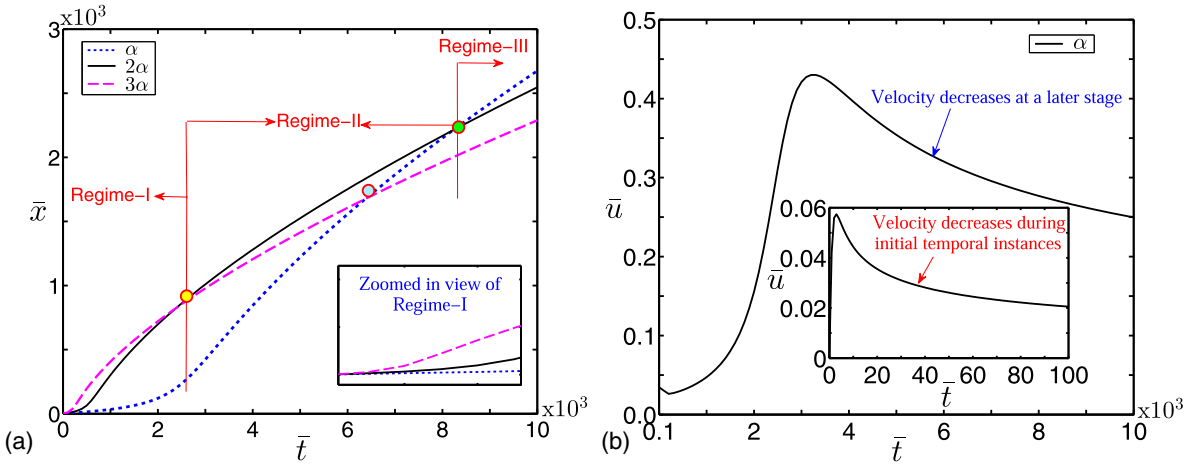

FIG. 3. (a) Plot showing the temporal variation of length of the liquid in the capillary, obtained for three different values of taper angle φ corresponding to $\alpha(=0.01)$, $2\alpha(=0.02)$, and $3\alpha(=0.03)$; (b) temporal variation of the velocity, obtained for taper angle φ corresponding to α. The other parameters considered for plotting are $\lambda = 0.01$ s, $\eta = 0.01$ Pa s, $\theta_s = 45^\circ$. The different regimes of imbibition are observed from the depicted variation. Inset shows the zoomed-in view of regime I.

erties, geometrical parameter of the flow configuration, and flow properties, and discuss their impact on the underlying fluid motion systematically in the forthcoming sections. Also, unless stated otherwise, we consider the following set of parameters in investigating the flow physics of our interest in this endeavor: $\alpha = 0.01$; $\epsilon = 1.0$; $\lambda = 0.01$ s; $\gamma_s = 0.1$ N/m; $\eta = 0.01$ Pa s; $\rho = 1000\,\mathrm{kg/m^3}$; $\theta_s = 45^\circ$; $\sigma = 0.01\,\mathrm{S^2/m^2}$; $R_I = 100\ \mu$m; [4]. It is worth mentioning here that a similar set of dimensional values is typical to the chosen fluidic setup and is used in the referred study as well [4,27].

A. Geometry of the flow configuration: Effect of taper angle

We begin our discussion with the temporal variation of filling length ($\bar{x}$ vs $\bar{t}$), as shown in Fig. 3(a), obtained for a change in the taper angle $\varphi(=\tan^{-1}\alpha)$. We compare our results for three different values of taper angle, corresponding to α, 2α, and 3α, where α is given as $\alpha = 0.01$. From the geometry of the chosen fluidic confinement (shown in Fig. 1), it is apparent that the outlet radius will increase with increasing the value of α. In the conical fluidic confinements, the filling time (which is defined as the time taken by the meniscus to reach a certain length of capillary) varies inversely with the tube radius at the position of the meniscus. However, we observe three distinct regimes of filling in Fig. 3(a). In this study, we consider different values of α by varying R_O. Now as R_O increases, signifying an increase in the magnitude of φ (as α becomes higher), the filling becomes much faster on account of higher surface tension force, which increases with increase in the radius, acting on the fluid mass being imbibed. This observation is apparent from regime I of Fig. 3(a).

We would like to add here that the present analysis focuses on the temporal variation of the filling length of a viscoelastic fluid following the imbibition dynamics. In the paradigm of spontaneous imbibition, a balance between the capillary and viscous forces is always retained [6,14]. At the beginning of imbibition, the fluid gets into the capillary from rest and under the influence of surface tension force only. This sudden impact leads to attain higher velocity of the fluid being imbibed as can be verified from the inset of Fig. 3(b). It is worth mentioning here that during this early stage, a very high shear rate developed due to a sudden rise in velocity resulting in an infinite effective viscosity in the process. This higher effective viscosity, which is induced during the early stage of the imbibition, increases the viscous resistance and, consequently, leads to a reduction in the velocity of the advancing fluid meniscus [cf. inset of Fig. 3(b)]. However, as time progresses, the meniscus of the advancing fluid (the fluid being imbibed) moves further down along the axial direction in the capillary making a balance between the capillary and viscous forces as supported by the increase in velocity in Fig. 3(b). Since, in the conical capillaries, as is the case for this analysis, the radius increases in the flow direction, the filling rate gets slowed down, attributed primarily to the mass conservation constraint (velocity will decrease) in the flow field. The phenomenon of reduction in flow velocity at a later stage of the process is witnessed in Fig. 3(b). Next, we discuss the three distinct regimes of filling as seen in Fig. 3(a) in greater detail.

In the present case, as already discussed, we keep R_I fixed (R_O is varied). Thus, an increase in R_O (signifying a higher α) will increase the degree of divergence of the fluidic channel chosen in this analysis. At the initial stages, since the fluid is being imbibed to the capillary from rest, the only driving force is the surface tension force. And since we have varied the outlet radius keeping the inlet radius constant, the force due to surface tension increases with increase in the radius and fluid in the capillary with greater α (equivalently, higher φ) attains higher velocity. Due to higher velocity, the underlying filling becomes faster for higher $\alpha(=2\alpha, 3\alpha)$ in regime I as seen in Fig. 3(a). Because of the relatively higher fluid velocity for higher values α, the imbibing fluid for these cases invites greater viscous resistance and due to the dominance of viscous forces over surface tension force at later stages (in regimes II and III), filling slows down. Also, for the higher values of α, at a later stage of filling, when the advancing fluid column starts occupying the divergent part of the conical capillary, the fluid velocity reduces upon satisfying the mass conservation constraint and culminating in a slow-down stage of the filling

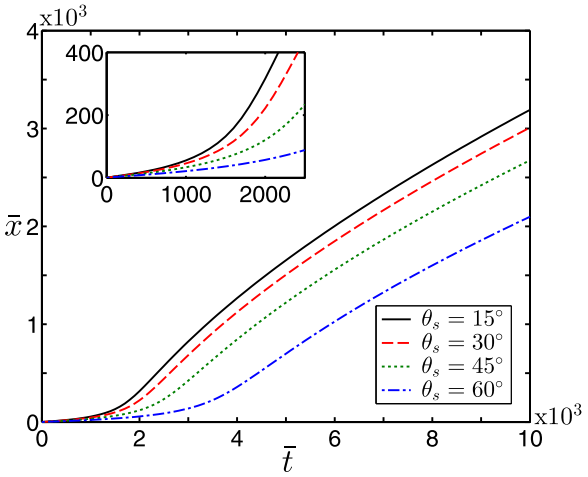

FIG. 4. The temporal variation of length of the liquid in the capillary, obtained for different values of contact (static) angle $\theta_s = 15°$, $30°$, $45°$, and $60°$. The other parameters considered for this plot are $\lambda = 0.01$ s, $\eta = 0.01$ Pa s, $\varphi = \tan^{-1}\alpha$. Inset shows the imbibition rate during initial stage. With increasing the magnitude of the static contact angle, the imbibition rate slows down.

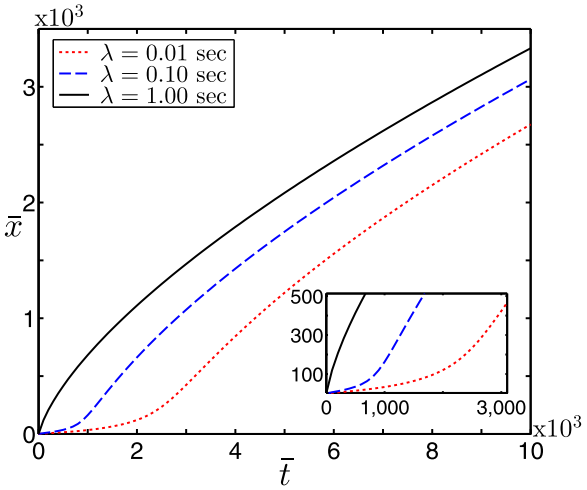

FIG. 5. Plot of the temporal variation of filling length in the capillary, obtained for different values of $\lambda = 0.01$ s, 0.10 s, and 1.0 s, respectively. The other parameters are $\eta = 0.01$ Pa s, $\varphi = \tan^{-1}\alpha$, $\theta_s = 45°$. Inset shows the imbibition rate during initial stage. As the magnitude of relaxation time λ becomes less, the filling time becomes larger.

process. These two effects altogether result in a slow-down of the filling process for higher values of α during late stages as observed in Fig. 3(a). On the other hand, to maintain a balance between capillary and viscous forces in the paradigm of spontaneous imbibition as is the case for this analysis, at later stages of the underlying process, the fluid in the capillary with smaller α fills at a faster rate. This can be explained using the fact that viscous force to act as a resistive force on the imbibing fluid column becomes least for smaller α due to the lesser velocity attained from a relatively lesser surface tension force during the initial regime (regime I). Also, on account of a lesser degree of divergence for a lesser value of α, at a later stage of filling, when the advancing fluid column starts occupying the divergent part of the conical capillary, the fluid velocity does not reduce appreciably and favors the filing. As such, it is because of these two effects that the filling time for smaller α is seen to be less than that of higher values of α. This phenomenon is observed in regime III of Fig. 3(a).

B. Effect of surface wettability

In Fig. 4, we demonstrate the filling length versus time obtained for different values of static contact angle $\theta_s = 15°$, $30°$, $45°$, and $60°$. As already mentioned, the filling length here refers to the temporal advancement of the invading fluid column along the axial direction of the channel. Induction of artificial effective viscosity due to the large shear rate at a very early instance of the imbibition phenomenon gives rise to an augmented viscous resistance to the flow of invading fluid (precisely at the contact line). It is because of this that the underlying filling process gets slowed down during the initial stage ($0 < \bar{t} < 1e3$) of the imbibition. A very lesser slope, i.e., nearly parallel nature of the curves depicting the temporal variation of filling, as witnessed by the inset of Fig. 4, underlines the slower rate of imbibition. On the other hand, at a later stage, we observe a relatively faster filling, attributed primarily to the balance between the prevailing forces, viz., the viscous force and the capillarity effect, of the imbibition dynamics [6]. Quite notably, a reduction in the static contact angle θ_s leads to an accelerated filling process, as is apparent from Fig. 4. With a reduction in θ_s (static contact angle), the wetting condition of the confining surface becomes progressively favorable towards the fluid being imbibed into the channel. This higher affinity of the surface towards the invading fluid triggers the imbibition phenomenon and quickness of the filling process, as witnessed in Fig. 4.

C. Fluid properties: Effect of relaxation time

As already mentioned, the fluid which is imbibed into the fluidic assay is viscoelastic. To explore the effect of viscoelasticity on the underlying imbibition dynamics, we plot, in Fig. 5, the temporal advancement of filling length in the fluidic assay for different values of relaxation time λ (= 0.01 s, 0.10 s, and 1.0 s). We note that at any temporal instant, the filling length in the channel increases with an increase in the relaxation time (λ) from 0.01 s to 1 s. This variation is attributed to the enhancement of the shear-thinning nature of the viscoelastic fluid with increasing the magnitude of λ. Here, λ, being the fluid relaxation time is an indicative measure of the elastic effect of the fluid. A relatively larger λ (higher relaxation time) signifies highly viscoelasticity of the fluid, and at times increases the fluid's shear-thinning nature. It is because of the increase in the shear-thinning nature with increasing the value of λ that the viscosity of fluid and its eventual impact in providing resistance to the imbibition process becomes less. Notably, following this reason, albeit all other conditions (boundary conditions, surface wettability, etc.) remain the same, on account of a relatively lesser resistance as realized at a higher relaxation time (λ), the invading fluid takes relatively less time to penetrate along the length of the capillary as witnessed by a smaller filling time in Fig. 5. Also, we

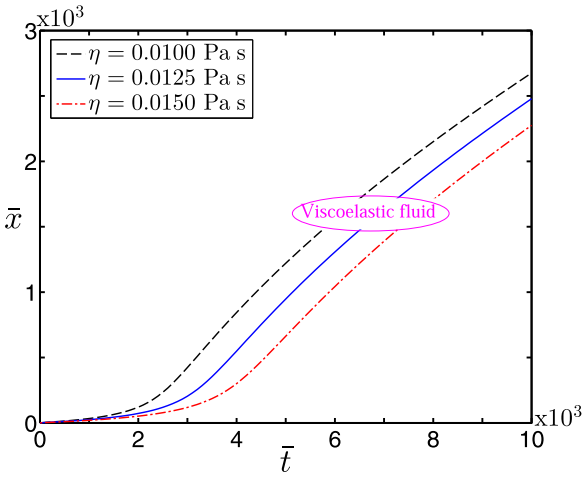

FIG. 6. Variation of filling length in the capillary versus time. The depicted plots are obtained for different values of $\eta =$ 0.01 Pa s, 0.0125 Pa s, and 0.0150 Pa s, respectively. The other parameters considered for this plot are $\lambda = 0.01$ s, $\varphi = \tan^{-1}\alpha$, $\theta_s =$ 45°. With increasing the magnitude of the apparent viscosity, the filling time becomes higher.

observe from Fig. 5 that at the early stage of the imbibition phenomenon $(0 < \bar{t} < 1e3)$, the curves for the relatively lesser values of λ (= 0.01 s, 0.10 s) are nearly parallel to the time axis, thus signifying a slow filling process. The slowing down effect of the imbibition phenomenon during the earlier stage of filling for the smaller values of λ(= 0.1 s, 0.01 s), which is mainly due to the high shear rate induced artificial viscosity effect, can be verified from the inset of Fig. 5.

D. Fluid properties: Effect of apparent viscosity

By depicting Fig. 6, we make an effort to bring about the effect of the apparent viscosity of the fluid (η) on the imbibition dynamics. It is worth mentioning here that the chosen values of η, as considered in plotting Fig. 6, conform to the typical values of several biofluids [4,27]. With increasing the magnitude of η from 0.01 Pa s (fluid rheology starts deviating and exhibits more viscoelastic behavior), the imbibition rate becomes slower as witnessed by a larger filling time in Fig. 6. Pertinent to the imbibition phenomenon in a capillary, an underlying balance between capillary pressure gradient and viscous pressure gradient is always retained. In the conical microfluidic channel, as time grows, the imbibition rate decreases due to the velocity reduction. Since velocity and its gradient decrease with time, the apparent viscosity will decrease with increasing temporal instant. No matter how the apparent viscosity decreases with time in the imbibition process, the elastic effect of the fluid for $\lambda = 0.01$ s will make the filling processes slow on account of slower response of the fluid to the driving force being applied in the process. However, this slow-down effect of the filling becomes more effective for higher η in the paradigm of spontaneous imbibition as seen in Fig. 6, attributed primarily to the higher viscous resistance to the process.

E. Imbibition dynamics: Scaling analysis

We show Fig. 7 to discuss the scaling estimation of the temporal variation of the filling length of the fluid being imbibed into the conical fluidic channel. The other parameters considered for the plot depicted in Fig. 7 are as follows: $\lambda = 0.01$ s, $\alpha = 0.01$, $\theta_s = 45°$. We observe from Fig. 7 three distinct regimes in which the imbibition dynamics follows different scaling laws.

In regimes I and III, the temporal variation of the filling length follows the 2/3 law, while in the intermediate regime, i.e., in regime II, the variation of the filling length ($\bar{x}$) with time ($\bar{t}$) follows nearly $\bar{x} \sim \bar{t}$ proportionality. At the beginning of the filling, the fluid imbibed into the channel upon experiencing a balance between the inertia and surface tension forces. From the fact that at initial stages, the only balancing force available is inertia forces as represented by the left-hand side in Eq. (15), we compare the scales of these two prominent forces (inertia force and surface tension force). As the result of the above comparison, we observe that variation of filing length vs time follows $\bar{x} \sim \bar{t}^{2/3}$ proportionally. It is worth mentioning here that at the initial stage of process, the fluidic channel builds up higher shear rates due to this force only. The higher shear rates lead to the induction of artificial apparent viscosity during this initial stage of imbibition and result in higher viscous drag acting at the contact line. So, initially, due to a more substantial effect due to viscous resistance applied at the contact line, the channel experiences a nonlinear variation of imbibition phenomenon as seen from regime I of Fig. 7. It is worth mentioning here that induction of artificial apparent viscosity during the earlier instant of imbibition, which leads to a reduction in velocity in regime I (see inset of Fig. 7), has already been discussed in one of the preceding sections.

After this initial regime (regime I), the underlying balance between capillary pressure gradient and viscous pressure gradient leads to a linear variation of the filling length ($\bar{x}$) with time ($\bar{t}$) as witnessed by a nearly $\bar{x} \sim \bar{t}$ proportionality in regime II of Fig. 7. As apparent from the inset of Fig. 7, the velocity in regime II increases and results in a higher velocity gradient as well. The higher velocity gradient will increase the magnitude of the viscous force acting at the contact line, and the balance between the dominant viscous and capillary forces offers a relatively faster filling following the linear scaling law in regime II. In regime III, on the other hand, we find the variation of filling length versus time to follow the 2/3 law, i.e., $\bar{x} \sim \bar{t}^{2/3}$. The attributable physical reasoning behind this variation is as follows: the variation in regime III refers to the late stage (at later temporal instances) of the imbibition dynamics. During later temporal instances, the imbibed fluid mass occupies a relatively larger flow area pertaining to the chosen fluidic assay and hence, the flow velocity decreases [cf. insets of Fig. 7 and Fig. 3(b)]. With a reduction in the flow velocity, the magnitude of the viscous force acting over the contact line reduces, attributed primarily to reducing the shear rate. Thus, the resulting balance between the dominant forces, i.e., the capillary and viscous forces, condenses the new filling regime wherein the variation of filling length ($\bar{x}$) with time ($\bar{t}$) follows $\bar{x} \sim \bar{t}^{2/3}$ proportionally. For the analysis of later stages, we use the least square fitting method to find the best fit straight line for the $\bar{x}$ *and* $\bar{t}$ data points on a log-log plot separately for both regimes. On analyzing the slope of the

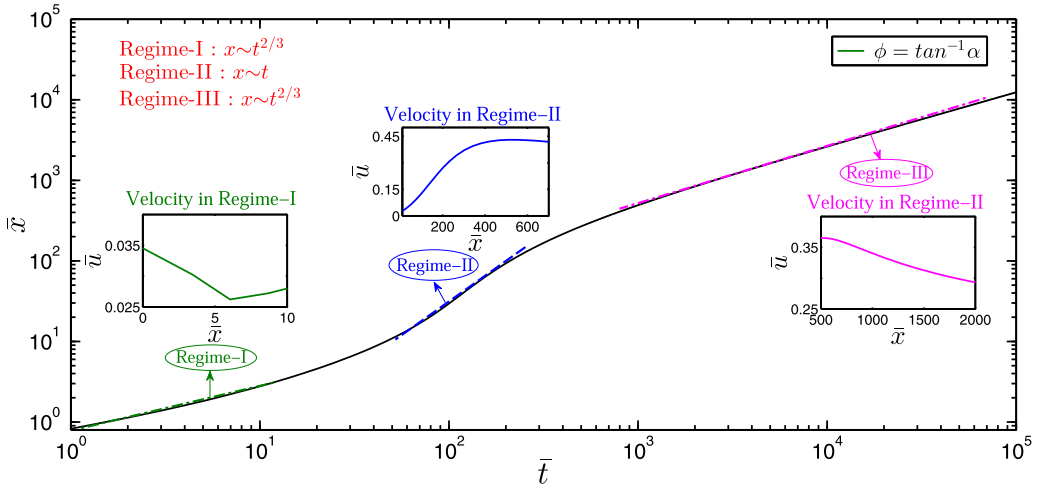

FIG. 7. Plot of the scaling analysis of the imbibition dynamics. Filling behavior in three different regimes is shown through the scaling estimate between the length of the liquid column imbibed into the capillary versus time. The depicted plots obtained for different parametric values pertinent to this analysis are $\lambda = 0.01$ s, $\varphi = \tan^{-1}\alpha$, $\theta_s = 45^\circ$ and $= 0.01$ Pa s.

straight lines obtained using this method, we deduce the proportionality relationship between filling length ($\bar{x}$) and time ($\bar{t}$) for regime II and regime III.

V. CONCLUSIONS

In this study, we have developed a theoretical model to describe imbibition dynamics of viscoelastic fluid in microfluidic assays having a nonuniform cross section. The analysis considers the sPTT model for describing the rheology of the viscoelastic fluid. The model accounts for the geometrical aspects of the fluidic assay and the rheological parameters characterizing the viscoelasticity of the fluid to describe the temporal evolution of the fluid in the assay in the capillary-driven regime. As verified by the satisfactory agreement of our model predictions against the established results reported in the literature, the developed theoretical framework can capture the underlying imbibition phenomenon, which is physically consistent with the operating regimes of chosen fluidic assay as well, quite effectively. The reported results of this study are nonintuitive and exciting as well. The significance of the results or inferences obtained from the present model includes identification of three different filling regimes in the conical microfluidic assay alongside the prediction of the scaling law for the identified regimes. A change in the shear rate as modulated by the nonuniformity of the cross section of the fluidic assay leads to an alteration in the viscous force in the flow process. And this spatiotemporal variation of the viscous force by tuning a balance with the capillary force in the paradigm of spontaneous imbibition results in three distinct filling regimes.

On the other hand, the present model seems to be of enormous relevance from the application viewpoint. Our model can be considered an effective tool for designing and optimizing the microfluidic assays, requiring a tradeoff between geometrical aspects of the fluidic device and fluid properties (rheological behavior). Precise optimization of these two aspects is essential for controlling the fluidic operation in biochemical and biomedical analysis where optimum filling time and the requirement of the minimal sample volume are necessary to provide augmented functionalities of the microfluidic assays, typically used for point-of-care diagnostics.

ACKNOWLEDGMENTS

P.K.M. gratefully acknowledges the financial support provided by the SERB (DST), India, through Project No. MTR/2020/000034. The authors greatly acknowledge Dr. H. S. Gaikwad for his help with the discussion pertaining to the analysis of capillary filling. The authors wish to express their gratitude to the anonymous reviewers for their insightful suggestions which helped to enhance the clarity of writing and discuss the results with more in-depth interpretation.

[1] E. W. Washburn, Phys. Rev. **17**, 273 (1921).
[2] B. M. Mognetti and J. M. Yeomans, Phys. Rev. E **80**, 056309 (2009).
[3] H. Kusumaatmaja, C. M. Pooley, S. Girardo, D. Pisignano, and J. M. Yeomans, Phys. Rev. E **77**, 067301 (2008).
[4] H. S. Gaikwad, A. Roy, and P. K. Mondal, J. Non-Newtonian Fluid Mech. **282**, 104317 (2020).
[5] W. Holloway, J. M. Aristoff, and H. A. Stone, Phys. Fluids **23**, 081701 (2011).
[6] S. R. Gorthi, S. K. Meher, G. Biswas, and P. K. Mondal, Proc. R. Soc. London, Ser. A **476**, 20200496 (2020).
[7] S. R. Gorthi, P. K. Mondal, G. Biswas, and K. C. Sahu, Can. J. Chem. Eng. **99**, 725 (2021).

[8] P. K. Mondal, U. Ghosh, A. Bandopadhyay, D. Dasgupta, and S. Chakraborty, Phys. Rev. E **88**, 023022 (2013).
[9] S. R. Gorthi, H. S. Gaikwad, P. K. Mondal, and G. Biswas, Ind. Eng. Chem. Res. **59**, 3839 (2020).
[10] D. DasGupta, P. K. Mondal, and S. Chakraborty, Phys. Rev. E **90**, 023011 (2014).
[11] M. S. Agrawal, H. S. Gaikwad, P. K. Mondal, and G. Biswas, Applied Mathematical Modelling **75**, 201 (2019).
[12] P. K. Mondal, D. DasGupta, and S. Chakraborty, Phys. Rev. E **90**, 013003 (2014).
[13] G. Kunti, P. K. Mondal, A. Bhattacharya, and S. Chakraborty, Phys. Fluids **30**, 092005 (2018).
[14] R. M. Digilov, Langmuir **24**, 13663 (2008).
[15] C. L. A. Berli and R. Urteaga, Microfluid. Nanofluid. **17**, 1079 (2014).
[16] S. Das, P. R. Waghmare, and S. K. Mitra, Phys. Rev. E **86**, 067301 (2012).
[17] S. Das and S. K. Mitra, Phys. Rev. E **87**, 063005 (2013).
[18] D. D. Joseph, *Fluid Dynamics of Viscoelastic Liquids* (Springer, New York, 1990).
[19] H. S. Gaikwad, P. Baghel, R. Sarma, and P. K. Mondal, Phys. Fluids **31**, 022006 (2019).
[20] S. Balasubramanian, P. Kaushik, and P. K. Mondal, Phys. Fluids **32**, 112003 (2020).
[21] C. G. Subramaniam and P. K. Mondal, Phys. Fluids **32**, 013108 (2020).
[22] P. K. Mondal, D. DasGupta, A. Bandopadhyay, U. Ghosh, and S. Chakraborty, Phys. Fluids **27**, 032109 (2015).
[23] P. K. Mondal, D. Dasgupta, and S. Chakraborty, Soft Matter **11**, 6692 (2015).
[24] S. Chakraborty, Anal. Chim. Acta **605**, 175 (2007).
[25] P. K. Mondal, D. DasGupta, A. Bandopadhyay, and S. Chakraborty, J. Appl. Phys. **116**, 084302 (2014).
[26] H. S. Gaikwad, G. Kumar, and P. K. Mondal, Soft Matter **16**, 6304 (2020).
[27] A. Bandopadhyay, U. Ghosh, and S. Chakraborty, Phys. Rev. E **89**, 053024 (2014).
[28] N. P. Thien and R. I. Tanner, J. Non-Newtonian Fluid Mech. **2**, 353 (1977).
[29] R. Sarma, N. Deka, K. Sarma, and P. K. Mondal, Phys. Fluids **30**, 062001 (2018).
[30] H. S. Gaikwad, D. N. Basu, and P. K. Mondal, Colloids Surf., A **518**, 166 (2017).
[31] P. K. Mondal, Transp. Porous Media **100**, 17 (2013).
[32] N. Phan-Thien, J. Rheol. (Melville, NY, U. S.) **22**, 259 (1978).
[33] L. L. Ferrás, A. M. Afonso, M. A. Alves, J. M. Nóbrega, and F. T. Pinho, Phys. Fluids **28**, 093102 (2016).